Fast Polynomial Approximation to Heat Diffusion in Manifolds

Shih-Gu Huang[1], Ilwoo Lyu[3], Anqi Qiu[2], Moo K. Chung[1]

[1]University of Wisconsin, Madison, USA
[2] National University of Singapore, Singapore
[3]Vanderbilt University, Nashville, USA

Abstract. Heat diffusion has been widely used in image processing for surface fairing, mesh regularization, surface data smoothing. We present a new fast and accurate numerical method to solve heat diffusion on curved surfaces. This is achieved by approximating heat kernel using high degree orthogonal polynomials in the spectral domain. The proposed polynomial expansion method avoids solving for the eigenfunctions of the Laplace-Beltrami operator, which are computationally costly for large mesh size, and the numerical instability associated with the finite element method based diffusion solvers. We apply the proposed method in localizing the male and female difference in cortical brain sulcal and gyral curve patterns.

1 Introduction

Heat diffusion has been widely used in image processing as a form of smoothing and noise reduction starting with Perona and Malik's ground breaking study [10]. Many techniques have been developed for surface fairing, mesh regularization, and surface data smoothing [1, 2, 3]. The diffusion equation has been solved by various numerical techniques. In [1, 2], the isotropic heat equation was solved by the least squares estimation of the Laplace-Beltrami (LB) operator and the finite difference method (FDM). In [3], the heat diffusion was solved iteratively by the discrete estimate of the LB-operator using the finite element method (FEM) and an FDM scheme. However, FDM schemes are known to suffer numerical instability if the sufficiently small step size is not chosen in the forward Euler scheme. In [11, 14], the LB-operator was used in the heat kernel convolution [3]. By constructing the heat kernel as a series expansion of the LB-eigenfunctions, the solution of the heat diffusion can be represented as a series expansion involving the LB-eigenfunctions. Although the LB-eigenfunction approach avoids the numerical instability associated with the FEM based diffusion solvers [3], the computational complexity is very high for large-scale surface meshes.

We propose a new fast and accurate numerical method to solve the heat diffusion by expanding the heat kernel using orthogonal polynomials. Taking advantage of recurrence relations of orthogonal polynomials [9], the computational run time of the proposed method is substantially reduced. We present three examples of the proposed methods based on the Chebyshev, Hermite and Laguerre polynomials. The proposed method is significantly faster than the LB-eigenfunction approach and FEM based diffusion solvers [3]. As an application, the proposed method is applied to a large number of magnetic resonance images (MRIs) to localize the sex differences in the sulcal and gyral patterns of the human cortical brain.

2 Preliminary

Suppose functional data f on surface $\mathcal{M} \in \mathbb{R}^3$ belong to $L^2(\mathcal{M})$, the space of square integrable functions on $\mathcal{M}$ with inner product $\langle f, h\rangle = \int_{\mathcal{M}} f(p)h(p)d\mu(p)$. $\mu(p)$ is the Lebesgue measure such that $\mu(\mathcal{M})$ is the total area of $\mathcal{M}$. Let Δ denote the LB-operator defined on $\mathcal{M}$. The isotropic heat diffusion equation on $\mathcal{M}$ with initial condition f is given by

$$\frac{\partial g(p,\sigma)}{\partial \sigma} + \Delta g = 0, \quad g(p, \sigma = 0) = f(p), \tag{1}$$

where σ is the diffusion time. It has been shown that the convolution of f with heat kernel K_σ is the unique solution of (1) [3],

$$g(p,\sigma) = K_\sigma * f(p) = \int_{\mathcal{M}} K_\sigma(p,q)f(q)dq.$$

Let ψ_j be the eigenfunctions of the LB-operator with eigenvalues λ_j, i.e., $\Delta\psi_j = \lambda_j\psi_j$. If we order the eigenvalues as $0 = \lambda_0 \leq \lambda_1 \leq \lambda_2 \leq \cdots$, the heat kernel can be expanded with exponential weight $e^{-\lambda\sigma}$ [3]: $K_\sigma(p,q) = \sum_{j=0}^{\infty} e^{-\lambda_j\sigma}\psi_j(p)\psi_j(q)$. Then, the heat diffusion can be expressed as

$$K_\sigma * f(p) = \sum_{j=0}^{\infty} e^{-\lambda_j\sigma} f_j\psi_j(p)$$

with coefficients $f_j = \int_{\mathcal{M}} f(p)\psi_j(p)d\mu(p)$.

3 Methods

We propose a new fast numerical method to solve the heat diffusion equation, bypassing the LB-eigenfunction computation and maintaining high accuracy. This is done by expanding the heat kernel using orthogonal polynomials such as the Chebyshev polynomials and their recurrence relations [9].

3.1 Heat diffusion using polynomial expansion

Consider an orthogonal polynomial basis P_n such as Chebyshev, Hermite and Laguerre polynomials, which is often defined by the following second order recurrence [9],

$$P_{n+1}(\lambda) = (\alpha_n\lambda + \beta_n)P_n(\lambda) + \gamma_n P_{n-1}(\lambda), \quad n \geq 0, \tag{2}$$

with initial conditions $P_{-1}(\lambda) = 0$ and $P_0(\lambda) = 1$. Assume P_n are orthogonal over interval $[a, b]$ with inner product $\int_a^b P_n(\lambda)P_k(\lambda)d\mu(\lambda) = \delta_{nk}$, the Dirac delta. We expand the exponential weight $e^{-\lambda\sigma}$ of the heat kernel as

$$e^{-\lambda\sigma} = \sum_{n=0}^{\infty} c_{\sigma,n} P_n(\lambda), \quad c_{\sigma,n} = \int_a^b e^{-\lambda\sigma} P_n(\lambda) d\mu(\lambda). \tag{3}$$

Using (3), the heat kernel convolution becomes

$$K_\sigma * f = \sum_{j=0}^{\infty} e^{-\lambda_j \sigma} f_j \psi_j = \sum_{n=0}^{\infty} c_{\sigma,n} \sum_{j=0}^{\infty} P_n(\lambda_j) f_j \psi_j.$$

Since $P_n(\lambda)$ is a polynomial of degree n, we have $P_n(\lambda_j)\psi_j = P_n(\Delta)\psi_j$, and

$$K_\sigma * f = \sum_{n=0}^{\infty} c_{\sigma,n} P_n(\Delta) f. \tag{4}$$

The direct computation of $P_n(\Delta) f$ requires the computation of $\Delta f, \cdots, \Delta^n f$, which is costly. Instead, we compute $P_n(\Delta) f$ by the following recurrence

$$P_{n+1}(\Delta) f = (\alpha_n \Delta + \beta_n) P_n(\Delta) f + \gamma_n P_{n-1}(\Delta) f, \quad n \geq 0,$$

with initial conditions $P_{-1}(\Delta)f = 0$ and $P_0(\Delta)f = f$. In the numerical implementation, we discretized the LB-operator using the cotan formulation [3, 14].

Chebyshev, Hermite and Laguerre expansion methods. We present three examples of the polynomial expansion methods based on the Chebyshev, Hermite and Laguerre polynomials, denoted by T_n, H_n and L_n respectively. The Chebyshev polynomials were used in the diffusion wavelet transform [7] and convolutional neural network on graphs [4]. Using the orthogonal conditions of the polynomials (Table. 1), we derive the closed-form expressions of the coefficients $c_{\sigma,n}$ (Table. 2) [6]. Note that T_n are orthogonal over the interval $[-1, 1]$, but $e^{-\lambda\sigma}$ ranges over $[0, \infty]$. Hence, in numerical implementation, given upper bound λ_{max} on the eigenvalues of the LB-operator, we expand $e^{-\lambda\sigma}$ for the interval $\lambda \in [0, \lambda_{max}]$ by $\overline{T}_n(\lambda) = T_n\left(\frac{2\lambda}{\lambda_{max}} - 1\right)$ [7, 4]. From the recurrence relations (Table. 1), $\overline{T}_n(\Delta)f$, $H_n(\Delta)f$ and $L_n(\Delta)f$ used in heat diffusion can be recursively computed by the relations given in Table. 2.

Figure 1 is an illustration of the heat diffusion of the left hippocampus surface mesh coordinates ($\sigma = 1.5$, $m = 100$). The reconstruction error is measured by the mean squared error (MSE) between the polynomial expansion method and the original surface mesh. Since the Chebyshev expansion method converges the fastest with the smallest error in various surface meshes, it will be used through the paper but other polynomial methods can be similarly applicable.

Iterative convolution. In the case we need the solutions of heat diffusion at multiple time points, instead of applying the polynomial expansion method with different σ, we can perform the iterative heat kernel convolution [3],

$$K_\sigma * f = \underbrace{K_{\sigma/m} * \cdot * K_{\sigma/m}}_{m \text{ times}} * f.$$

Table 1: Orthogonal conditions and recurrence relations of polynomials [9].

Polynomials	Orthogonal conditions	Recurrence relations[‡]
Chebyshev	$\int_{-1}^{1} T_n(\lambda)T_k(\lambda)\frac{1}{\sqrt{1-\lambda^2}}d\lambda = \frac{(1+\delta_{n0})\pi}{2}\delta_{nk}$	$T_{n+1}(\lambda) = (2-\delta_{n0})\lambda T_n(\lambda) - T_{n-1}(\lambda)$
Hermite	$\int_{-\infty}^{\infty} H_n(\lambda)H_k(\lambda)e^{-\lambda^2}d\lambda = \sqrt{\pi}2^n n!\delta_{nk}$	$H_{n+1}(\lambda) = 2\lambda H_n(\lambda) - 2nH_{n-1}(\lambda)$
Laguerre	$\int_{0}^{\infty} L_n(\lambda)L_k(\lambda)e^{-\lambda}d\lambda = \delta_{nk}$	$L_{n+1}(\lambda) = \frac{(2n+1-\lambda)L_n(\lambda) - nL_{n-1}(\lambda)}{n+1}$

[‡]The initial conditions of all polynomials are $P_{-1}(\lambda) = 0$ and $P_0(\lambda) = 1$, where $P = T$, H or L.

Table 2: Coefficients and recurrence relations of polynomial expansion methods.

Method	Coefficients $c_{\sigma,n}$	Recurrence relations[‡]
Chebyshev[†]	$(-1)^n(2-\delta_{n0})e^{-\frac{\lambda_{max}}{2}\sigma} \cdot I_n(\lambda_{max}\sigma/2)$	$\overline{T}_{n+1}(\Delta)f = (2-\delta_{n0})\left(\frac{2\Delta}{\lambda_{\max}} - 1\right)\overline{T}_n(\Delta)f - \overline{T}_{n-1}(\Delta)f$
Hermite	$\frac{1}{n!}\left(\frac{-\sigma}{2}\right)^n e^{\frac{\sigma^2}{4}}$	$H_{n+1}(\Delta)f = 2\Delta H_n(\Delta)f - 2nH_{n-1}(\Delta)f.$
Laguerre	$\frac{\sigma^n}{(\sigma+1)^{n+1}}$	$L_{n+1}(\Delta)f = \frac{(2n+1-\Delta)L_n(\Delta)f - nL_{n-1}(\Delta)f}{n+1}$

[†]I_n are the modified Bessel functions of the first kind [9].
[‡]The initial conditions of all methods are $P_{-1}(\Delta)f = 0$ and $P_0(\Delta)f = f$, where $P = \overline{T}$, H or L.

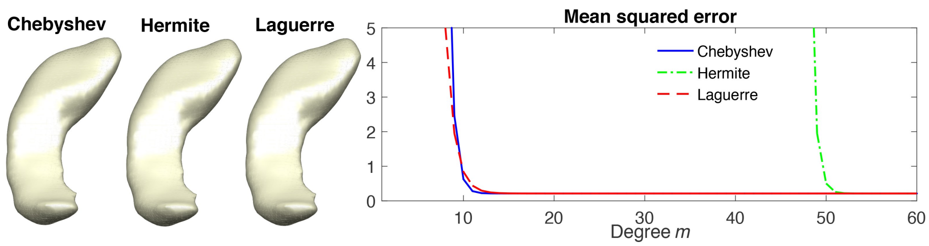

Fig. 1: Left: heat diffusion with $\sigma = 1.5$ using the Chebyshev, Hermite and Laguerre polynomial expansion methods with degree $m = 100$. Right: MSE between the original surface mesh and the polynomial expansion methods for different m. The Chebyshev method converges the fastest in general.

For example, if we computed $K_{0.25} * f$, then $K_{0.5} * f$ is simply computed as two repeated kernel convolution $K_{0.25} * (K_{0.25} * f)$, and diffusion with much larger diffusion time can be done similarly. Figure 2 displays heat diffusion with $\sigma = 0.25$, 0.5, 0.75 and 1 realized by iteratively applying the Chebyshev expansion method with $\sigma = 0.25$ sequentially four times.

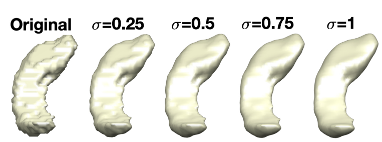

Fig. 2: Sequential application of Chebyshev expansion method with $\sigma = 0.25$ four times.

3.2 Validation

We compared the Chebyshev expansion method against the FEM based diffusion solver and the LB-eigenfunction approach [3] on the unit spheres with

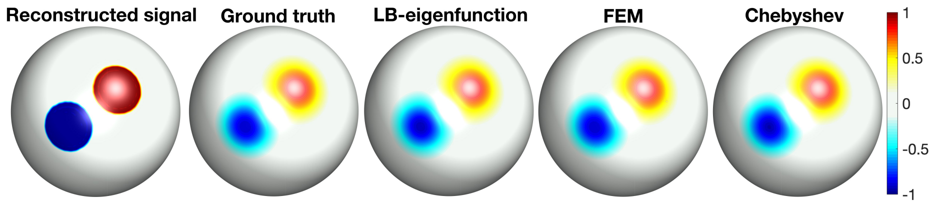

Fig. 3: Reconstructed signal and ground truth of heat diffusion with $\sigma = 0.01$ are constructed by the SPHARM representation with degree 100. The LB-eigenfunction approach with 210 eigenfunctions, FEM based diffusion solver with 405 iterations, and Chebyshev expansion method with degree 45 have similar accuracy, MSE at around 10^{-5} against the ground truth.

2562, 10242, 40962 and 163842 mesh vertices. On the unit spheres, the ground truth of heat diffusion can be analytically constructed by the spherical harmonics (SPHARM), which is the LB-eigenfunctions [3]. Consider the surface signal consisting of values 1, -1 and 0 that was expanded by the SPHARM [12] with degree 100, which is taken as the initial condition of heat diffusion. The ground truth was then constructed using the SPHARM coefficients. The Chebyshev expansion method along with LB-eigenfunction approach and FEM-based diffusion solvers were applied to the spherical mesh in solving the heat diffusion. Figure 3 shows the result with $\sigma = 0.01$ on the unit sphere with 163842 vertices.

Run time over mesh sizes. For fixed σ, the FEM based diffusion solver and Chebyshev expansion method need more iterations and higher degree for larger meshes, while the LB-eigenfunction approach is nearly unaffected by the mesh sizes (Figure 4-left). Since there is a trade-off between the accuracy and computational run time, we fixed the numerical accuracy with MSE at around 10^{-5} and compared the run time (Figure 4-right).

Run time over diffusion times. For fixed mesh resolution, the FEM based diffusion solver and Chebyshev expansion method need more iterations and higher degree for larger σ, while the LB-eigenfunction approach requires less number of eigenfunctions (Figure 5-left). Figure 5-right displays the computational run time versus σ with MSE at around 10^{-7}.

From Figure 4-left and Figure 5-left, we can see that the accuracy of the proposed method and LB-eigenfunction approach increases gradually with the expansion degree and number of eigenfunctions, while the FEM based diffusion solver remains a low accuracy until the number of iterations is large enough. At similar accuracy, the LB-eigenfunction approach is the slowest, and the proposed method is up to 12 times faster than the FEM based diffusion solver (Figures 4-right and 5-right).

4 Application

The proposed method was applied to perform heat diffusion on the inner brain surface to measure the relative distance between sulcal and gyral curves. If sulcal and gyral curves are in close proximity, heat will diffuse faster.

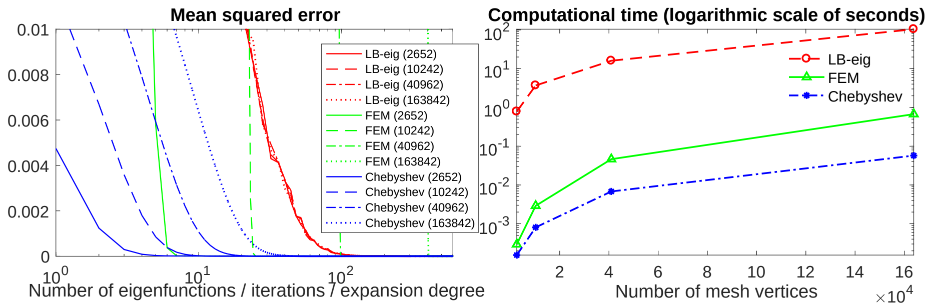

Fig. 4: Left: MSE of the LB-eigenfunction approach, FEM based diffusion solver and Chebyshev expansion method against the ground truth with different number of eigenfunctions, iterations and expansion degree respectively. Unit spheres with 2562, 10242, 40962 and 163842 mesh vertices and fixed $\sigma = 0.01$ were used. Right: computational run time versus mesh size for MSE at around 10^{-5}.

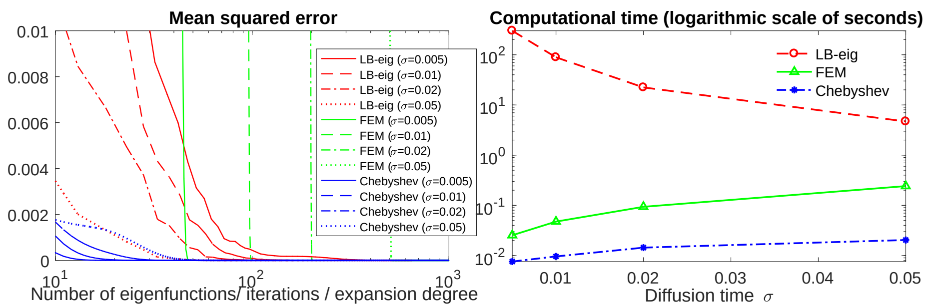

Fig. 5: Left: MSE of the LB-eigenfunction approach, FEM based diffusion solver and Chebyshev expansion method against the ground truth with different number of eigenfunctions, iterations and expansion degree respectively. Diffusion times $\sigma = 0.005$, 0.01, 0.02 and 0.05 and fixed mesh resolution (40962 vertices) were used. Right: computational run time versus σ for MSE at around 10^{-7}.

Preprocessing. We used the T1-weighted MRI dataset consisting of 269 females and 177 males. The MRI data underwent structural preprocessing including distortion correction, image alignment and nonlinear registration to the MNI template, and white matter and pial surface mesh extractions by FreeSurfer.

The automatic sulcal curve extraction method [8] was used to detect concave regions (sulcal fundi). Sulcal points were determined by the line simplification method [5] that denoises the sulcal regions. A partially connected graph was constructed by the sulcal points, where edge weights are assigned based on geodesic distances. Finally, the sulcal curves were traced over the graph. Similarly, gyral curves were extracted by finding convex regions.

Diffusion maps. We assigned the gyral curves value 1, sulcal curves value -1, and all other parts value 0 (Figure 6). We used the Chebyshev expansion method with diffusion time $\sigma = 0.001$ and expansion degree $m = 1000$. On

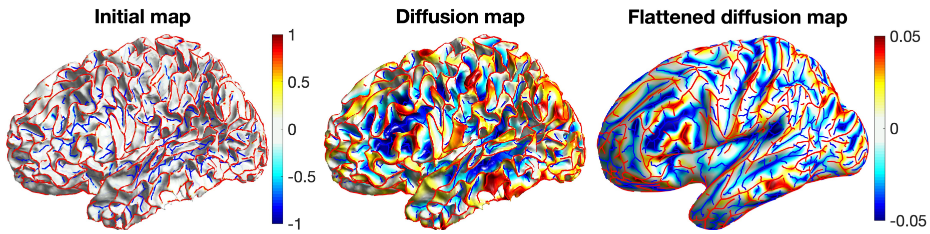

Fig. 6: Left: sulcal (blue) and gyral (red) curves are extracted and displayed along the white matter surface. Middle: heat diffusion using the Chebyshev expansion method with expansion degree 1000 and diffusion time 0.001. Right: diffusion map was flattened to show the pattern of diffusion.

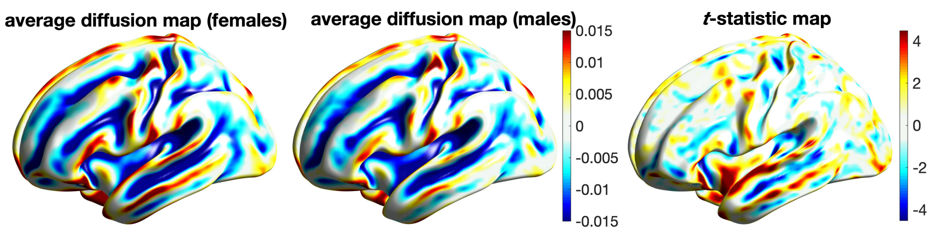

Fig. 7: Left and middle: average diffusion maps of 269 females and 177 males displayed on the average surface template. Right: t-statistic map shows localized sulcal and gyral pattern differences (female-male) thresholded at -4.51 and 4.49.

average, the construction of the discrete LB-operator took 3.19 seconds and the Chebyshev expansion method took 1.78 seconds resulting in a total run time of 4.97 seconds per subject in a computer.

Statistical analysis. The average diffusion maps of females and males in Figure 7 show major differences in the temporal lobe among other regions, which is responsible for processing sensory input into derived meanings for the appropriate retention of visual memory, language comprehension, and emotion association [13]. The two-sample t-statistic map was constructed on the diffusion maps (max. t-stat 7.14, min. t-stat -6.99). We performed permutation test with half million permutations and obtained the empirical null distribution of maximum and minimum t-statistics for multiple comparisons. t-statistic values larger than 4.49 and smaller than -4.51 give the corrected p-values below 0.05.

5 Conclusion

In this paper, we proposed a new fast and accurate numerical method to solve heat diffusion on curved surfaces by expanding the heat kernel in the spectral domain by orthogonal polynomials. The proposed method avoids the computation of LB-eigenfunctions, which are computationally costly for large scale meshes and the numerical instability in FEM based diffusion solvers with the forward scheme. At the similar high numerical accuracy, the proposed method is significantly faster than the LB-eigenfunction approach and even faster than the FEM based diffusion solver. The proposed method was applied to compute heat diffusion on the brain surfaces, requiring only 4.97 seconds per subject in localizing the male and female difference in sulcal and gyral curve patterns.

References

1. A. Andrade, F. Kherif, J. Mangin, K.J. Worsley, A. Paradis, O. Simon, S. Dehaene, D. Le Bihan, and J-B. Poline. Detection of fMRI activation using cortical surface mapping. *Human Brain Mapping*, 12:79–93, 2001.
2. A. Cachia, J.-F. Mangin, D. Riviére, D. Papadopoulos-Orfanos, F. Kherif, I. Bloch, and J. Régis. A generic framework for parcellation of the cortical surface into gyri using geodesic Voronoï diagrams. *Image Analysis*, 7:403–416, 2003.
3. M.K. Chung, A. Qiu, S. Seo, and H.K. Vorperian. Unified heat kernel regression for diffusion, kernel smoothing and wavelets on manifolds and its application to mandible growth modeling in CT images. *Medical Image Analysis*, 22:63–76, 2015.
4. M. Defferrard, X. Bresson, and P. Vandergheynst. Convolutional neural networks on graphs with fast localized spectral filtering. In *Advances in Neural Information Processing Systems*, pages 3844–3852, 2016.
5. D.H. Douglas and T.K. Peucker. Algorithms for the reduction of the number of points required to represent a digitized line or its caricature. *Cartographica: The International Journal for Geographic Information and Geovisualization*, 10:112–122, 1973.
6. I.S. Gradshteyn and I.M. Ryzhik. *Table of integrals, series, and products, 7th ed.* San Diego, CA: Academic, 2007.
7. D.K. Hammond, P. Vandergheynst, and R. Gribonval. Wavelets on graphs via spectral graph theory. *Applied and Computational Harmonic Analysis*, 30:129–150, 2011.
8. I. Lyu, S. Kim, N. Woodward, M. Styner, and B. Landman. TRACE: A topological graph representation for automatic sulcal curve extraction. *IEEE Transactions on Medical Imaging*, 37(7):1653–1663, 2018.
9. F.W.J. Olver, D.W. Lozier, R.F. Boisvert, and C.W. Clark. *NIST handbook of mathematical functions.* Cambridge University Press, 2010.
10. P. Perona and J. Malik. Scale-space and edge detection using anisotropic diffusion. *IEEE Trans. Pattern Analysis and Machine Intelligence*, 12:629–639, 1990.
11. M. Reuter. Hierarchical shape segmentation and registration via topological features of Laplace-Beltrami eigenfunctions. *International Journal of Computer Vision*, 89:287–308, 2010.
12. L. Shen, J. Ford, F. Makedon, and A. Saykin. Surface-based approach for classification of 3D neuroanatomical structures. *Intelligent Data Analysis*, 8:519–542, 2004.
13. B. Smith, M. Ashburner, C. Rosse, J. Bard, W. Bug, W. Ceusters, L.J. Goldberg, K. Eilbeck, A. Ireland, and C.J. Mungall. The OBO foundry: coordinated evolution of ontologies to support biomedical data integration. *Nature Biotechnology*, 25:1251, 2007.
14. M. Tan and A. Qiu. Spectral Laplace-Beltrami wavelets with applications in medical images. *IEEE Transactions on Medical Imaging*, 34:1005–1017, 2015.